Analysis and Characterization of Traveling-Wave Electrode in Electroabsorption Modulator for Radio-on-Fiber Application

Jiyoun Lim, Young-Shik Kang, Kwang-Seong Choi, Jong-Hyun Lee, Sung-Bock Kim, and Jeha Kim, *Associate Member, IEEE*

***Abstract*—Comparing with a lumped electroabsorption modulator (EAM), we show the merits of a long EAM with traveling-wave electrode with high radio-frequency (RF) gain that could be used in high-frequency analog application. By terminating the RF output port with the characteristic impedance of 30 Ω, the device exhibited a large enhancement of 6 dB above 10 GHz in the electrical-to-optical response and a wide fractional bandwidth as estimated from simulation. In addition, an input impedance matching circuit of stub embedded on the device chip was found to be very effective for improving RF characteristics in the narrow band of frequency.**

***Index Terms*—Electroabsorption modulators, electroabsorption modulator with traveling-wave electrode (TWEAM), impedance matching, radio-on-fiber, traveling wave electrode.**

I. Introduction

THE electroabsorption modulator with traveling-wave electrode (TWEAM) was initially proposed to overcome the bandwidth limitation of the lumped electroabsorption modulator (EAM) [1]. Although velocity matching is not easy to accomplish with InP material [2], a TWEAM is still very attractive for many applications, especially at high frequency. There have been some reports on this device's use as an optical time-division-multiplexed demultiplexing and detecting device [3] and a short pulse generator [4]. Recently, many reports on the wireless fiber-optic link have been presented and paid much attention in anticipation for the last mile solution of the broadband access network [5]–[7]. However, few reports on TWEAM for narrow-band application such as radio-on-fiber (ROF) exist. Focusing on a limited range of frequency band, TWEAM needs not only a new approach to the RF termination but also the proper impedance matching scheme.

In this paper, we investigated TWEAM modules in terms of the proper termination and the matching scheme. The fabrication of the devices and modules is presented in Section II and their characterization in Section III. In Section IV, we discuss the electrical properties relating traveling-wave electrodes and investigated the performance enhancement of the modules by both the output termination and the input impedance matching circuits.

Manuscript received April 24, 2003; revised August 20, 2003.

The authors are with the Electronics and Telecommunications Research Institute, Daejeon, Korea.

Digital Object Identifier 10.1109/JLT.2003.821740

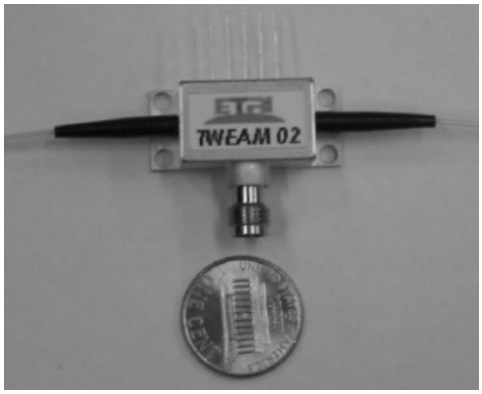

Fig. 1. Fabricated TWEAM module.

II. TWEAM Device and Module

The frequency response of TWEAM is related to structural parameters such as the epi and the electrode structure. Since the epi structure directly affects the high-frequency response, not to mention the extinction ratio [8], the epilayer was carefully designed through the finite-difference time-domain simulation. A 0.5-μm-thick n^+ layer grown on a semi-insulating InP substrate was designed for slow wave mode operation. A 0.3-μm of intrinsic layer contained the strain compensated multiple quantum well (MQW) structure, which consisted of 13 pairs of wells (10 nm, −0.38% tensile strained) and barriers (7 nm, 0.5% compressive strained). The photoluminescence peak was at 1.50 μm.

To study the effect of electrode on the response, we prepared three types of devices with 100-, 200-, and 300-μm-long active waveguide for comparison. The width of the active waveguide was 2 μm. At each side of the active waveguide there was a 250-μm-long passive waveguide butt-jointed. For high-frequency operation, we employed the coplanar waveguide (CPW) electrode and formed it by evaporation. It was varied in both the width of signal electrode and the gap between signal and ground electrodes. In addition, devices with lumped electrodes were also prepared to prove the merit of a traveling-wave electrode at high frequency. The details of the device fabrication process were presented elsewhere [9].

TWEAM modules were assembled in a butterfly-type housing with a V-connector as shown in Fig. 1. A CPW electrode patterned alumina submount was located between the V-connector and a TWEAM device chip. Due to its strong influence on the frequency response, the submount was carefully designed through HFSS simulation in such a way that it had

0733-8724/03$17.00 © 2003 IEEE

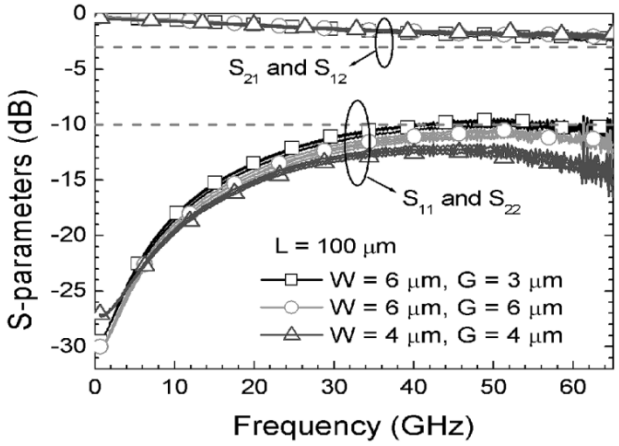

Fig. 2. S-parameters of fabricated TWEAM chips with various traveling-wave electrode structures.

as low an electrical return loss as possible over a wide range of frequency. In the full two-port S-parameter measurement, we observed that S_{11} of the submount was kept below -10 dB at frequencies lower than 37.4 GHz while S_{21} was above -3 dB at high frequencies up to 35 GHz [10]. A 50-Ω thin-film resistor formed on an alumina substrate was used to terminate RF power. The submount, the device chip, and the resistor were interconnected with 2-mil-wide gold ribbons. Finally, a tapered optical fiber was actively aligned at each facet of the device.

III. Device Characterization

TWEAM modules for digital and analog applications differ not by the device chip but by an impedance matching scheme. Thus, we studied the characteristics of chips used in broadband modules. For comparison, we prepared three kinds of CPW electrode, which differed in the width of signal electrode and in the gap between signal and ground electrodes. We observed the return loss S_{11} and the insertion loss S_{21} from the devices of 100-μm length as presented in Fig. 2. It was found that the S_{11} of the devices became small with the narrow electrode width. For a given width, the device exhibited lower return loss with the wider gap. Since a narrow electrode width and a wide gap means high characteristic impedance in CPW structure, these results agreed well with the fact that the characteristic impedance of InP TWEAM was lower than 50 Ω [2]. On the other hand, the insertion loss S_{21} was observed to be less than -2.5 dB in the range of frequency up to 65 GHz for all the electrode structures.

Fig. 3 is the Dc electrical-to-optical transmission characteristics of the modules. The transfer curve in Fig. 3(a) shows high Dc extinction ratio of 28 and 38 dB at -2 V bias voltage for the modules of 100- and 200-μm-long devices, respectively. The devices revealed optimized operation at 1550 nm. Even though the optical insertion loss at 0 V was slightly higher at 1550 nm than at 1570 nm, the Dc extinction at -2 V was much higher by more than 10 dB regardless of the device length. On the other hand, the slope efficiency η of the transfer curve is an important parameter particularly in analog application, which is directly related with RF link gain in ROF system [11]. It is given

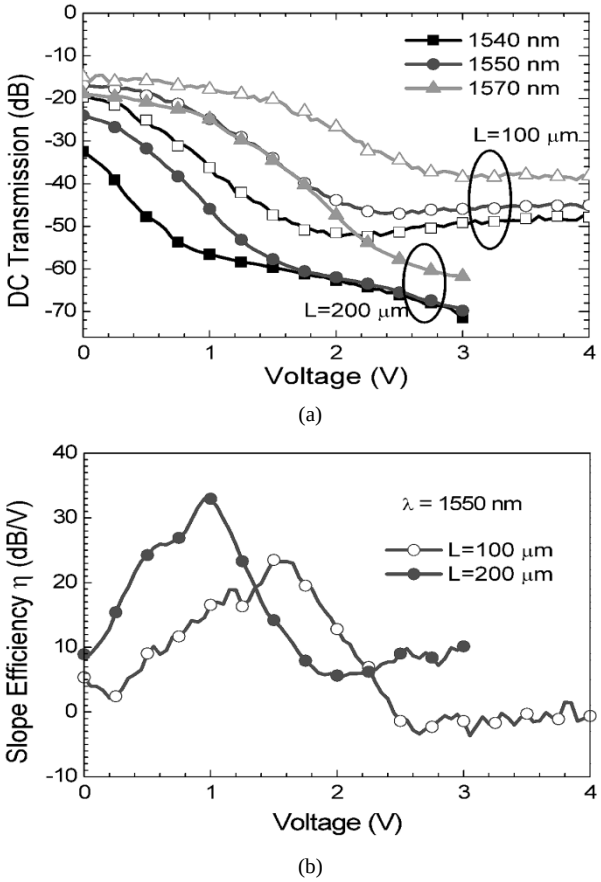

Fig. 3. DC transmission characteristics of modules (a) transfer curves and (b) slope efficiency η.

as the derivative of transfer function T_{dB} with respect to the bias voltage V as follows:

$$\eta = -\frac{dT_{dB}}{dV}. \tag{1}$$

Fig. 3(b) shows the slope efficiency at 1550 nm. As the device was long, the maximum gain became large at low bias voltage.

Electrical-to-optical (E/O) frequency response was measured using an Anritsu 37 397C vector network analyzer and a photodetector with known frequency response. Fig. 4 shows the small signal E/O responses of the modules of 100- and 200-μm -long devices measured at the wavelengths of 1550 nm with various bias voltages. The modules were packaged with the same submount and with 50-Ω termination. The resonances at 24 and 39 GHz in the response were observed for both devices of 100 and 200 μm and they were proved to be the microstrip (MSL) mode-like parallel plate (PPL) mode [12] through HFSS simulation. The PPL mode was generated by the phase delay induced in the CPW waveguide of input submount and causes power leakage in the waveguide. It could be significantly suppressed by packaging schemes. In addition, we observed the frequency rolloff in the response at low frequency below 3 GHz. There are origins presented for the feature such as the imperfect passive optical waveguide [13] and the impedance mismatching between the electrode and the probing pad. Considering the device fabrication [9], we believe that the frequency rolloff resulted from the impedance mismatching at the tapered region of

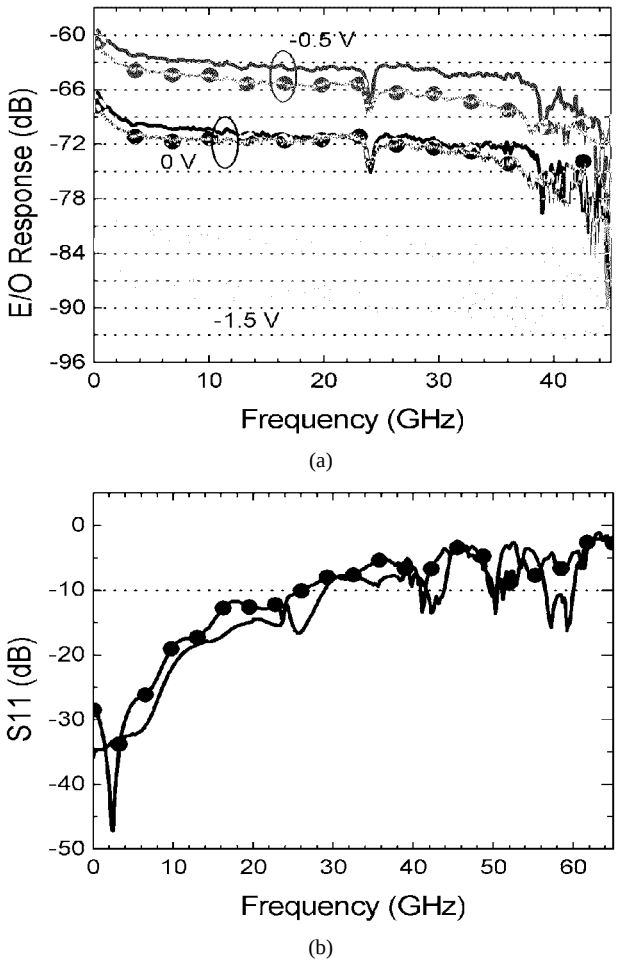

Fig. 4. E/O response of modules of 100- (line) and 200-μm-long (symbol line) devices.

electrode. Excluding the low-frequency rolloff, the small signal 3-dB bandwidth was about 38 and 32 GHz for the modules of 100- and 200-μm-long devices, respectively.

IV. TWEAM in ROF Application

In the following, we describe some approaches to design an analog EAM associated with a traveling-wave electrode. To begin with, we investigated the electrical properties of a TWEAM compared with a lumped EAM in order to verify its traveling-wave effect. Then the RF termination matched to the characteristic impedance of the device and the embedded matching circuit were considered as the methods of accommodating TWEAM modules for analog application

A. Traveling-Wave Effect in TWEAM

When a waveguide device is a considerable fraction of an RF wavelength in size, it is regarded as a transmission line with constant characteristic impedance rather than a lumped element. In such a device, the return loss S_{11} is not increased with the frequency beyond a certain limit value, unlike a capacitive device. Its specific behavior is mainly determined by the impedance matching with a load [8].

To investigate weather a TWEAM operates in a similar way to a transmission line, we compared the electrical response of the

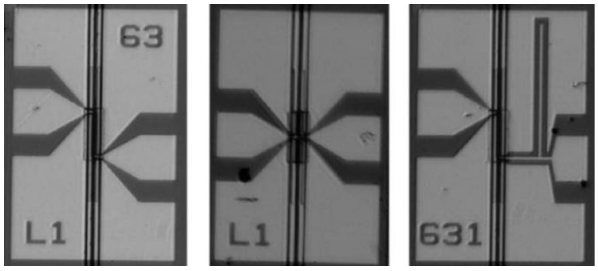

Fig. 5. Fabricated devices with (a) traveling-wave electrode, (b) lumped electrode, and (c) traveling-wave electrode with stub.

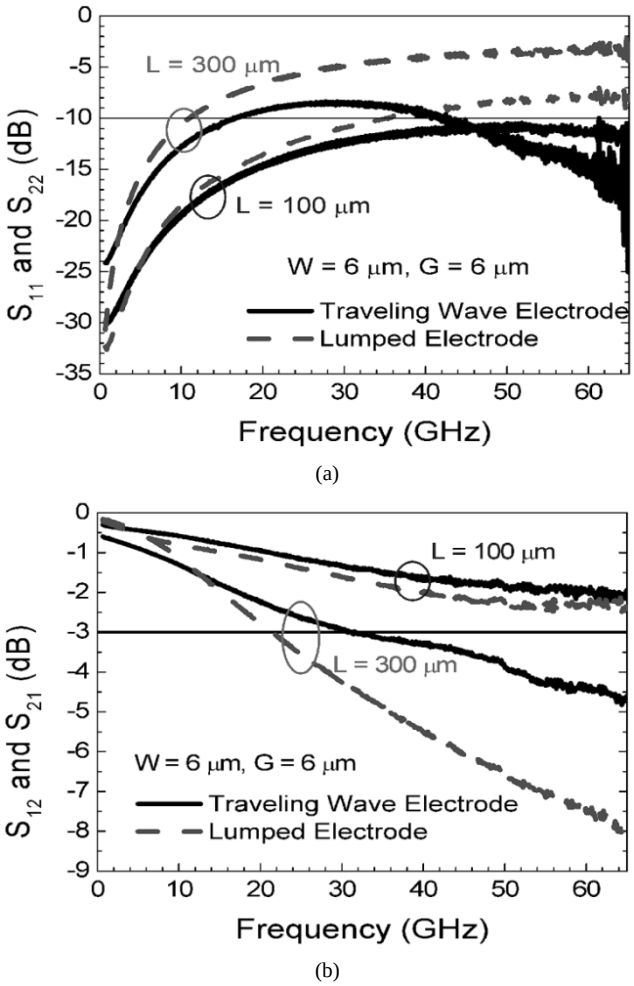

Fig. 6. Comparison of S-parameters of the devices with traveling wave electrode and lumped electrode. (a) S_{11} and S_{22}; (b) S_{12} and S_{21}.

devices with a traveling wave and a lumped electrode shown in Fig. 5(a) and (b). The lumped device was assumed to have the same capacitance as the one with a traveling-wave electrode because it was fabricated with the identical optical waveguide and the same passivation structures. The devices of 100- and 300-μm length were prepared for the study. For all types of devices, the CPW electrode consisted of an electrode strip width of 6 μm and a gap distance of 3 μm.

Fig. 6 shows measured S_{11} and S_{22}, and S_{21} and S_{12} of the devices. Despite the same device capacitance for both lumped EAM and TWEAM, as the frequency increased, S_{11} of TWEAMs decreased at high frequency while that of lumped

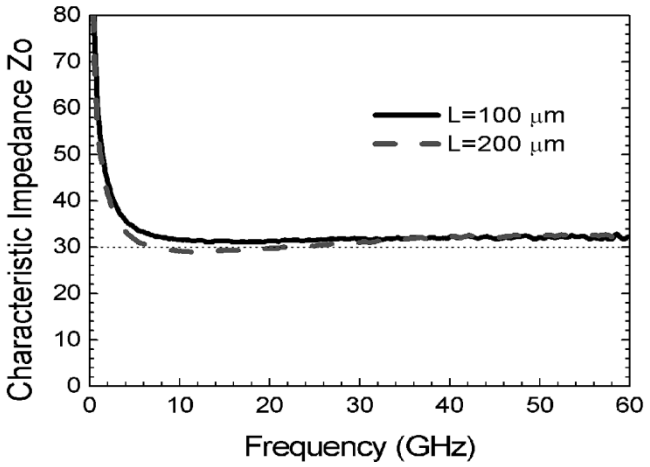

Fig. 7. Characteristic impedance of the devices with 100- and 200-μm-long electrode.

devices monotonically increased as usual. It showed a distinctive feature in the high frequency and varied markedly with the device length. At 60 GHz, the difference of S_{11} between the lumped EAM and the TWEAM of 300 μm was as large as 12 dB compared to a mere 5 dB for 100 μm. The behavior of S_{21} reflected the feature of S_{11}. The decline of S_{21} of the lumped device of 300 μm with respect to TWEAM was drastic up to 3 dB, while it deviated only by 0.5 dB for 100 μm. The rapid drop of S_{21} in the 300-μm device was attributed to the device capacitance.

The observation indicates that for a given device capacitance, a TWEAM yields low return loss at relatively high frequency and eventually provides better RF power transfer in the frequency compared with a lumped device. The transmission-line-like properties are significant even for the device with only a few hundred micrometer long traveling-wave electrode at the frequency above a few tens of gigahertz. At the high frequency near 60 GHz, it is easier for traveling-wave electrode structure to achieve low return loss with a long device up to 300 μm. With the high RF slope efficiency of a long waveguide device as described in Section III, it is advantageous to use TWEAM not only for digital application but also for analog application.

B. RF Termination

In broadband digital applications, the terminating impedance of TWEAM was proposed to be lower than 50 Ω [2], [14], and its broad frequency response was estimated with a termination matched to the characteristic impedance of the chip [15]. If we carefully design a TWEAM that operates in slow wave mode, it is possible to obtain constant characteristic impedance at high-frequency region [8]. Fig. 7 shows the characteristic impedance calculated from the measured S-parameters of the fabricated chips as a function of frequency. The characteristic impedance was about 30 Ω regardless of the device length.

In order to study the response of the impedance matched TWEAM, a submodule was prepared with a 100-μm-long chip and a 30-Ω thin-film resistor. RF signal was directly applied through an on-wafer probe to the chip without both an input

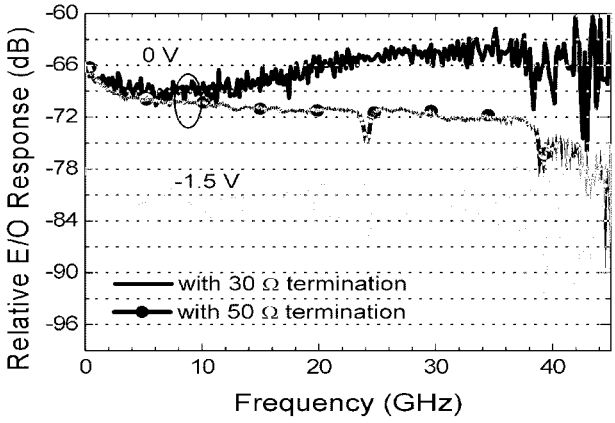

(a)

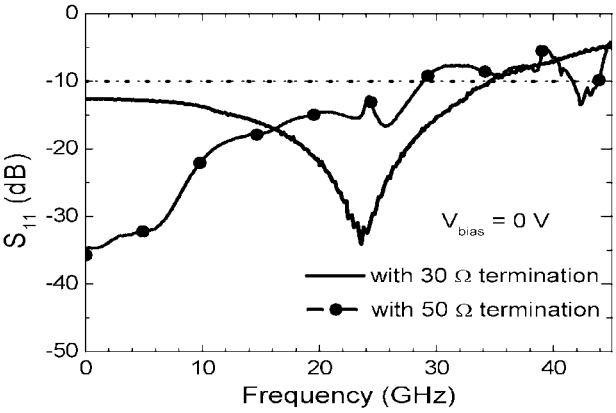

(b)

Fig. 8. (a) E/O response and (b) S_{11} of a TWEAM with both a 30- and 50-Ω termination.

RF submount and a connector. Fig. 8 shows the relative E/O response and the S_{11} observed in the submodule, and the results for the module with a 100-μm-long chip and a 50-Ω termination is included for comparison. Unlike the module tested in Section III, no resonance was observed in the E/O response of the submodule. This is because the submodule without input submount induced no phase delay. The TWEAM with 30-Ω termination showed a distinctive behavior in the E/O response and S_{11}, compared with the module with 50 Ω. Even though the reflection S_{11} was relatively high at low frequency, the E/O response showed a large enhancement of more than 6 dB in the frequency range above 10 GHz due to the low return loss at around 25 GHz. Our observation implies that in a given device, we could obtain improved response at high frequencies by proper characteristic impedance matching.

In addition to the enhancement of the E/O response, from the viewpoint of bandwidth, it is highly desirable to obtain the termination matched to the characteristic impedance of TWEAM. In principle, any value of termination could be used for an analog TWEAM, as long as the reflection at the RF input port is sufficiently suppressed with matching electronics at the frequency of concern. The termination, however, affects the design of an input impedance matching circuit and eventually determines the fractional bandwidth of the module. There is a parameter known as the Q of the circuit, which is the ratio of

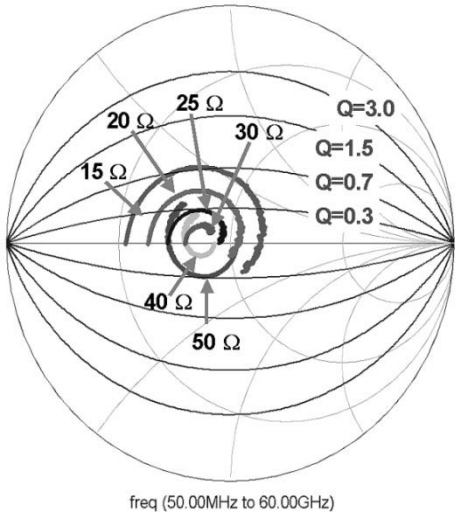

Fig. 9. Calculated S_{11} of a 100-μm-long TWEAM device with various terminating resistors.

the center frequency f_o to the fractional bandwidth according to [16]

$$Q = \frac{f_O}{\text{fractional bandwidth}}. \tag{2}$$

For a given center frequency, the lower the value of Q is, the wider the fractional bandwidth becomes. Fig. 9 shows the S_{11} simulated using measured device parameters with various terminating resistors assuming no impedance matching electronics at the input port. Constant Q contours were also drawn on the Smith chart. When we design the input impedance matching circuit, we try to move a point on the loci at the frequency of interest toward the center of the Smith chart. The trace of the point should be remained in the low Q region to achieve the wide fractional bandwidth. In Fig. 9, the loci for the devices with a termination less than 30 Ω showed behaviors of rotating clockwise toward the center of the Smith chart or the matching point as the frequency increased. Among others, the loci of the 30-Ω termination was located in low Q region less than 0.3 in the entire frequency range of 50 MHz to 60 GHz. According to our calculation, it was the best to have the TWEAM matched with a 30-Ω termination for achieving a wide fractional bandwidth. The result implies that the characteristic impedance matching at the output of TWEAM is of particular importance to the analog device.

C. Embedded Impedance Matching Circuit

After determining a proper RF output termination, impedance matching electronics at the input RF port of the device should be designed to transport the maximum signal power from an outside signal source to the module. The impedance matching circuit on an input submount is usually employed. The circuit is constructed with balancing capacitors of stub for the accurate impedance adjustment [17]. However, the trimming of the stubs with a laser is neither simple nor cost-effective. Therefore, it is worth employing the impedance matching circuit embedded in a device chip as the most possible alternative.

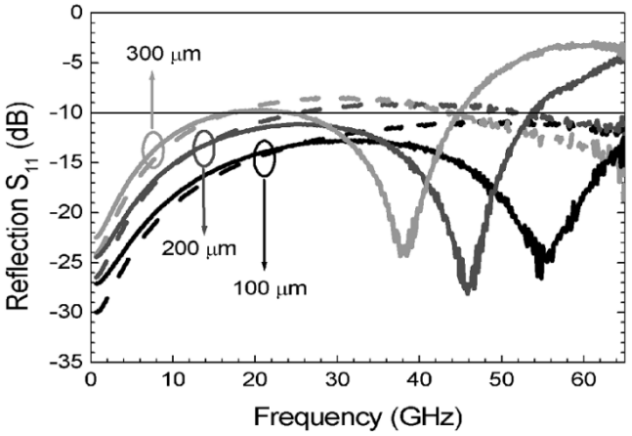

Fig. 10. S_{11} of devices: (solid) with and (dashed) without stub.

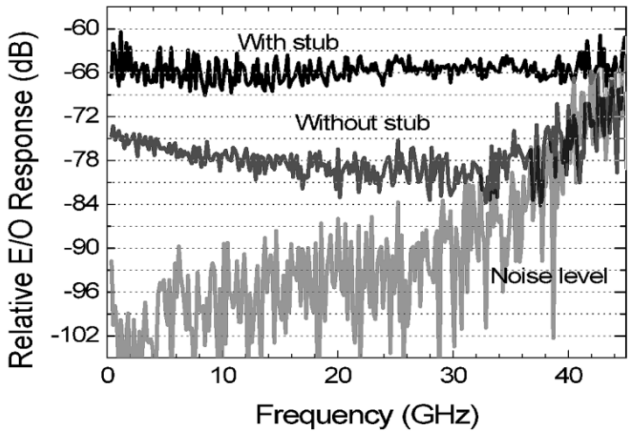

Fig. 11. E/O response of the devices with and without stub.

We fabricated devices with an asymmetric shunt stub at the RF input port as shown in Fig. 5(c) [18]. Fig. 10 shows the measured S_{11} of the TWEAMs with and without the stub circuit. The dips in S_{11} were shown at the frequency of 38, 46, and 55 GHz for devices of 300, 200, and 100 μm length, respectively. The relative E/O response shown in Fig. 11 was measured with the 100-μm-long devices from on-wafer probing. The terminating resistance was 50 Ω. We found that the response of the device with the stub showed an enhancement at the frequency over 10 GHz and maintained the gain up to 40 GHz, whereas it gradually decreased with the frequency for the device without the stub. About 5 dB was the E/O response improved at 30 GHz. The experiment suggests that the impedance matching stubs embedded in the device are very helpful for the high-frequency characteristics of TWEAM in terms of S_{11} and the E/O response.

V. Conclusion

We proposed and demonstrated a TWEAM as a very promising device for high-frequency analog applications such as an ROF system. Comparing with a lumped electrode EAM, a long TWEAM showed a high RF gain and a low RF return loss at high frequency. We found that unlike a lumped EAM, TWEAM should be thought of as a transmission line even for

a device only a few hundred micrometers in length. For our TWEAM, characteristic impedance matching of 30 Ω proved to be very important to obtain an improvement of E/O response and a wide fractional bandwidth. In addition, the impedance matching circuit formed with a stub embedded in the device would be a very effective way of improving the high-frequency response in narrow-band frequency.

REFERENCES

[1] K. Kawano, M. Kohtoku, M. Ueki, T. Ito, S. Kondoh, Y. Noguchi, and Y. Hasumi, "Polarization-insensitive traveling-wave electrode electroabsorption (TW-EA) modulator with bandwidth over 50 GHz and driving voltage less than 2 V," *Electron. Lett.*, vol. 33, pp. 1580–1581, Aug. 1997.

[2] G. L. Li, S. K. Sun, S. A. Pappert, W. X. Chen, and P. K. L. Yu, "Ultrahigh-speed traveling-wave electroabsorption modulator—Design and analysis," *IEEE Trans. Microwave Theory Tech.*, vol. 47, pp. 1177–1183, July 1999.

[3] V. Kaman, A. J. Keating, S. Z. Zhang, and J. E. Bowers, "Simultaneous OTDM demultiplexing and detection using an electroabsorption modulator," *IEEE Photon. Technol. Lett.*, vol. 12, pp. 711–713, June 2000.

[4] V. Kaman, Y.-J. Chiu, T. Liljeberg, S. Z. Zhang, and J. E. Bowers, "Integrated tandem traveling-wave electroabsorption modulators for $> 100\ \mathrm{Gbit/s}$ OTDM applications," *IEEE Photon. Technol. Lett.*, vol. 12, pp. 1471–1473, Nov. 2000.

[5] C. Lim, A. Nirmalathas, M. Attygalle, D. Novak, and R. Waterhouse, "The merging of a WDM fiber-radio backbone with a 25 GHz WDM ring network," in *IEEE MTT-S Int. Microwave Symp. Dig.*, vol. 1, 2003, pp. 273–276.

[6] K. Ikeda, T. Kuri, and K. Kitayama, "Simultaneous 3-band modulation 2.5-Gb/s baseband, microwave-, and 60-GHz-band signals using a single electroabsorption modulator for radio-on-fiber systems," in *IEEE MTT-S Int. Microwave Symp. Dig.*, vol. 1, 2003, pp. 261–264.

[7] T. Kuri, H. Toda, and K. Kitayama, "Dense wavelength-division multiplexing millimeter-wave-band radio-on-fiber signal transmission with photonic downconversion," *J. Lightwave Technol.*, vol. 21, pp. 1510–1517, June 2003.

[8] H. H. Liao, X. B. Mei, K. K. Loi, C. W. Tu, P. M. Asbeck, and W. S. C. Chang, "Microwave structures for traveling-wave MQW electro-absorption modulators for wide band 1.3 μm photonic link," in *Proc. SPIE Optoelectron. Integrated Circuits Conf.*, vol. 3006, 1997, pp. 291–300.

[9] Y.-S. Kang, J. Lim, S.-B. Kim, Y.-D. Chung, and J. Kim, "Fabrication of polarization insensitive electroabsorption modulator with traveling-wave electrode (TWEAM)," in *Proc. Korea-Japan Joint Workshop Microwave Millimeter Wave Photon.*, 2003, pp. 117–120.

[10] J. Lim, Y.-S. Kang, K.-S. Choi, J.-H. Lee, S.-W. Ryu, and J. Kim, "Fabrication and characterization of 20 GHz electroabsorption modulator module," in *Proc. Korea-Japan Joint Workshop Microwave Millimeter Wave Photon.*, 2003, pp. 49–52.

[11] R. B. Welstand, S. A. Pappert, D. T. Nichols, L. J. Lembo, Y. Z. Liu, and P. K. L. Yu, "Enhancement in electroabsorption waveguide modulator slope efficiency at high optical power," *IEEE Photon. Technol. Lett.*, vol. 10, pp. 961–963, July 1998.

[12] C.-C. Tien, C.-K. C. Tzuang, S. T. Peng, and C.-C. Chang, "Transmission characteristics of finite-width conductor-backed coplanar waveguide," *IEEE Trans. Microwave Theory Tech.*, vol. 41, pp. 1616–1624, Sept. 1993.

[13] G. L. Li, S. A. Pappert, P. Mages, C. K. Sun, W. S. C. Chang, and P. K. L. Yu, "High-saturation high-speed traveling-wave InGaAsP-InP electroabsorption modulator," *IEEE Photon. Technol. Lett.*, vol. 13, pp. 1076–1078, Oct. 2001.

[14] S. Z. Zhang, Y.-J. Chiu, P. Abraham, and J. E. Bower, "25 GHz polarization-insensitive electro-absorption modulators with traveling-wave electrodes," *IEEE Photon. Technol. Lett.*, vol. 11, pp. 191–193, Feb. 1999.

[15] J. Lim, S. Jeon, J. Kim, and S. Hong, "A circuit model of traveling wave electroabsorption modulator," in *IEEE MTT-S Int. Microwave Symp. Dig.*, vol. 3, 2002, pp. 1707–1710.

[16] G. Gonzalez, *Microwave Transistor Amplifiers Analysis and Design*. Englewood Cliffs, NJ: Prentice-Hall, 1997, ch. 2.

[17] N. Mineo, K. Nagai, and T. Ushikubo, "Ultra wide-band electroabsorption modulator modules for DC to millimeter-wave band," in *Int. Topical Meeting Microwave Photon.*, 2002, pp. 9–12.

[18] N. I. Dib, G. E. Ponchak, and L. P. B. Katehi, "A theoretical and experimental study of coplanar waveguide shunt stubs," *IEEE Trans. Microwave Theory Tech.*, vol. 41, pp. 38–44, Jan. 1993.

Jiyoun Lim received the B.S., M.S., and Ph.D. degrees in electrical engineering and computer science from Korea Advanced Institute of Science and Technology, Daejeon, in 1995, 1997, and 2002, respectively.

Since 1995, she has worked on the simulation and the fabrication of semiconductor optical devices. In 2002, she joined the Electronics and Telecommunications Research Institute, Daejeon, Korea, where she is a Senior Researcher. She is currently involved in a project on a 60-GHz analog optical modulator. Her research interests are the design and characterization of high-speed optoelectronic devices.

Young-Shik Kang received the B.S. degree in physics from Chungnam National University, Daejeon, Korea, in 1998 and the M.S. degree in information and communications from Kwangju Institute of Science and Technology, Kwangju, Korea, in 2000.

He joined the integrated optical source team as an Investigator in a project on a 60-GHz analog optical modulator and transceiver module for RF/optic conversion at the Electronics and Telecommunications Research Institute, Daejeon, Korea, in 2001. He currently carries out research on high-speed and linear multiple quantum-well optical modulators.

Kwang-Seong Choi received the B.S. degree in material science and engineering from Hanyang University, Korea, in 1993 and the M.S. degree in electronic material science from the Korea Advanced Institute of Science and Technology, Daejeon, in 1995.

From 1995 to 2001, he developed lead frame type CSPs, BLP packages, and stack packages with improving their solder joint reliability and designed high-speed electronic packages for DDR, Rambus DRAM, and RF device for Hynix Semiconductor. He has been a Senior Research Engineer at the Electronics and Telecommunications Research Institute, Korea, since 2001, where he has been designing high-speed photonic modules over 10 GHz with electrical simulation and measurement.

Jong-Hyun Lee received the B.S., M.S., and Ph.D. degree in metallurgical engineering and materials science from Hong Ik University, Seoul, Korea, in 1995, 1997, and 2001, respectively.

His doctoral work was the electronic packaging process and soldering for SMT. He is currently a Senior Researcher in the Basic Research Lab at the Electronics and Telecommunication Research Institute. His research interests include the fabricating process for optoelectronic modules and flip-chip bonding.

Dr. Lee is a member of IMAPS and TMS.

Sung-Bock Kim (A'03) was born in Daejeon, Korea, in 1965. He received the B.S. and M.S. degrees in physics from Yonsei University, Seoul, Korea, in 1990 and 1992, respectively.

In 1993, he joined the Electronics and Telecommunication Research Institute, Daejeon, as a Member of Research Staff in the Basic Research Laboratory. With a research background with compound semiconductor epitaxy growth, he is currently studying the optoelectronic materials and photonics devices grown by MOCVD.

Jeha Kim received the B.S. and M.S. degrees from Sogang University, Seoul, Korea, in 1982 and 1985, respectively, and the Ph.D. degree from the University of Arizona, Tucson, in 1993, all in physics.

He joined the Electronics and Telecommunications Research Institute, Daejeon, Korea, in 1993, where he worked in the Optoelectronics Section in the development of a 10-Gbit/s laser diode for optical communications. During 1995–1998, he worked on the high-temperature superconducting (HTS) passive and active microwave devices for high-sensitivity wireless communications. His current research interests are in the development of functional optoelectronic devices for WDM and OTDM fiber-optic communications and radio-on-fiber (ROF) link wireless system. He is now the Team Leader of the integrated optical source team and a Principal Investigator in the projects of hybrid integrated wavelength-selectable WDM optical source module and 60-GHz analog optical modulator and transceiver module for RF/optic conversion.